Segregation and formation of MnP particles during rapid thermal annealing of Mn-implanted InP and GaP

I. G. Bucsa,[a] R. W. Cochrane, and S. Roorda
Département de Physique and Regroupement Québécois sur les Matériaux de Pointe, Université de Montréal, CP 6128, Succursale Centre-Ville, Montreal, Quebec H3C 3J7, Canada

(Received 23 January 2009; accepted 8 June 2009; published online 15 July 2009)

We have studied the structural and magnetic properties of Mn implanted ($1-5\times10^{16}$ cm^{-2}, 200 keV) into InP and GaP substrates, before and after rapid thermal annealing. As revealed by Rutherford backscattering spectrometry, secondary ion mass spectrometry, and transmission electron microscopy measurements, implantation results in an amorphous surface layer 300 nm deep, and subsequent annealing gives rise to epitaxial recrystallization of this layer accompanied by a segregation of most of the Mn into clusters about 60 nm in diameter at the surface. Magnetic measurements indicate ferromagnetic behavior only for the annealed samples with T_C close to 290 K, characteristic of bulk MnP, whose presence is confirmed by diffraction data. In addition, there is no evident dependence of the magnetic and structural properties on the doping type or level of the substrates. © *2009 American Institute of Physics*. [DOI: 10.1063/1.3168448]

I. INTRODUCTION

Over the past decade much experimental[1–5] and theoretical[6–8] research has been carried out in an effort to produce ferromagnetic semiconductors for application in spintronic devices.[9] In this regard, III-V semiconductors doped with a few percent of magnetic ions, notably Mn, have been the target of much of this work following theoretical models[6] predicting ferromagnetism up to and beyond room temperature. Data on alloys produced by molecular beam epitaxy (MBE), metal-organic chemical vapor deposition (MOCVD), ion implantation, and thermal diffusion have been reported in GaAs,[1,3,10] InAs,[2] GaP,[4] InP,[5,11] GaP,[12] and GaN,[13] but often with conflicting results. MBE materials grown at relatively low temperatures (~300 °C) result in a homogeneous structure and show clear evidence of Mn substitution into the host lattice as well as uniform magnetic semiconductor behavior. Materials, particularly III-P alloys, produced at temperatures above 600 °C, however, are usually structurally and magnetically heterogeneous due to the limited equilibrium solubility of Mn in the host compound.[14–16]

In this paper, we clarify the formation process and the nature of the heterogeneous alloys formed by relatively high-energy Mn-ion implantation into InP and GaP, followed by rapid annealing above 600 °C. Our results are unambiguous: Mn implantation at room temperature, using an ion energy of 200 keV, amorphizes a surface layer several hundred nanometer thick. Rapid thermal annealing (RTA) results in a recrystallization of this layer, coherent with the substrate, and a concomitant segregation of a large fraction of the Mn to a narrow surface region about 60 nm wide. This segregation of the Mn at the surface results in the formation of nanometer-sized MnP grains, as clearly demonstrated by magnetic and diffraction data. The MnP grains exhibit magnetic behavior very similar to those of MnP clusters in MOCVD GaMnP,[14,15] and of bulk MnP, which is a highly anisotropic ferromagnet.[17]

II. EXPERIMENTAL DETAILS

InP(001) substrates, S-doped (*n*-type with $n\sim10^{19}$ cm^{-3}), Fe-doped (semi-insulating, $p\sim10^{16}$ cm^{-3}), Zn-doped (*p*-type with $p\sim5\times10^{17}$ cm^{-3}), and undoped, were implanted with Mn ions at fluences between 1×10^{16} and 5×10^{16} cm^{-2} and energies up to 200 keV using the 1.7 MV Tandetron accelerator on the Université de Montréal campus. Additionally, an *n*-type GaP(001) sample ($n\sim5\times10^{17}$ cm^{-3}) was implanted with 3×10^{16} Mn^{+}/cm^{2}.

After initial characterization, samples were subjected to a RTA in order to repair the implantation damage. In the case of InP, it has been found that an annealing temperature of more than 550 °C is necessary for recrystallization and incorporation of impurities into the InP, and more than 800 °C for a complete recovery of the matrix from defects.[18,19] In the experiments reported here, InP annealing temperatures have been limited to the range between 600 and 650 °C for 30–60 s. In contrast, the GaP sample was annealed at 750 °C. In all cases, the annealing was done under a nitrogen flow using samples mounted face-to-face with a piece of the substrate material to hinder oxidation and to protect against phosphorus loss.

Rutherford backscattering spectrometry (RBS) was carried out with a 2 MeV He beam using a detector situated at an angle of 10° with respect to the incident beam. Samples were mounted on a computer-controlled three-axis goniometer in order to perform measurements along both channeling—InP(001)—and random directions.

Atomic concentration profiles were measured before and after annealing by secondary ion mass spectrometry (SIMS) using an IONTOF-TOF.SIMS IV spectrometer. In order to calibrate the depth scale, the depth of the sputtered crater at the end of the SIMS analysis was measured with a Dek-Tak

[a]Electronic mail: ig.bucsa@umontreal.ca.

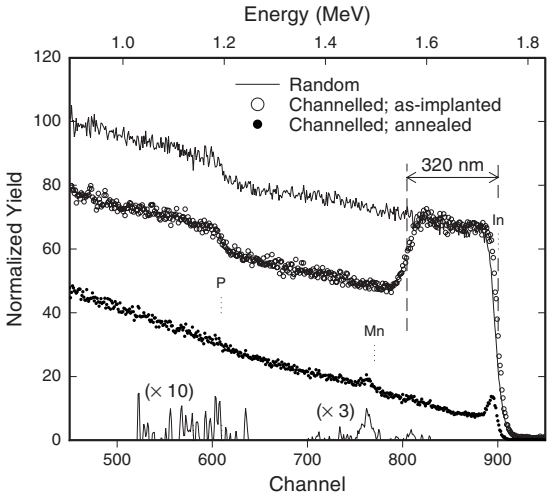

FIG. 1. RBS measurements for an InP(Fe) sample implanted with Mn to a total fluence of 2×10^{16} cm^{-2}; the solid line traces the spectrum for the as-implanted sample in a random direction, the open circles are for the as-implanted sample in the [001] channeling direction, and the filled circles are for the sample annealed for 60 s at 650 °C also in the [001] direction. The energetic positions of In, P, and Mn are indicated in the figure. At the bottom of the figure are the magnified peaks for Mn and P for the annealed, channeled spectrum after subtraction of the background.

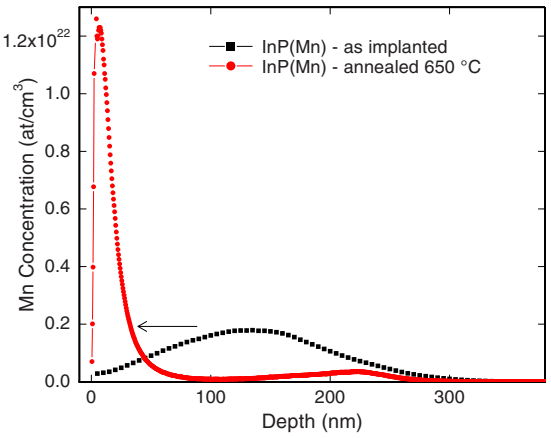

FIG. 2. (Color online) SIMS profiles of Mn-implanted InP(Fe) before annealing (squares) and after RTA at 650 °C for 1 min (circles). The arrow indicates the evolution of the Mn profile during annealing.

profilometer. Subsequently, the measured Mn profile was normalized by equating the integrated concentration to the implanted fluence.

Transmission electron microscopy (TEM) analyses were performed on a JEOL 2100F microscope equipped with a field-emission electron source operated at 200 kV. This instrument is also equipped with an x-ray detector capable of energy dispersive x-ray (EDS) mapping of the samples with the microscope in the scanning mode. Bright field, dark field, and also cross-sectional scanning TEM (STEM) images were taken.

Magnetic moment data were measured with a commercial (ADE Technologies) vibrating sample magnetometer (VSM) at fields up to 22.5 kOe and temperatures between 100 and 350 K.

III. EXPERIMENTAL RESULTS

A. RBS

Figure 1 shows the RBS spectra for the as-implanted sample with incident beam aligned along a random off-axis direction and also for the beam aligned along the (001) substrate axis. The high yield at all energies for the first spectrum is similar to that produced by an amorphous layer of the same composition. The second spectrum is interpreted as arising from an amorphous layer 320 (±10) nm thick at the surface of a crystalline substrate. This conclusion is also supported by x-ray diffraction measurements which show the substrate (200) and (400) peaks with an amorphous background. The indicated thickness of the amorphous layer corresponds to the penetration depth of 200 keV Mn ions in InP, as simulated by the TRIM[20] code.

After the RTA treatment, the spectrum in the channeling direction indicates epitaxial recrystallization of the implanted layer. Furthermore, a small peak for Mn is noted in this curve: numerical simulations with the RUMP[21] code suggest that the position and the small width of this peak are due to the accumulation of Mn at the surface of the sample. The integrated intensity of this peak represents approximately 80% of the implanted Mn fluence; this indicates that a certain amount of Mn is incorporated in the InP lattice or is located in a lattice coherent with the substrate.

B. SIMS

SIMS Mn-concentration profiles of an InP(Fe) sample, as-implanted at 200 keV with a fluence of 3×10^{16} cm^{-2} and after annealing at 650 °C, are presented in Fig. 2. The profile for the as-implanted sample has a Gaussian shape that fits well with Monte Carlo simulations produced with the TRIM code. The maximum concentration of 1.9×10^{21} at./cm^3 at 140 nm from the surface corresponds to a concentration of 4.5 at. % in InP; the average Mn concentration in the 320 nm implanted layer is calculated to be 2.5 at. %.

Annealing for 60 s at 650 °C produces a dramatic redistribution of the Mn atoms toward the surface of the recrystallized matrix, as shown in Fig. 2. Such segregation into a surface layer is not unexpected for an impurity with a low solubility subjected to planar crystallization.[22] Similar segregation of the Mn atoms to the surface was found for all implanted and annealed substrates: semi-insulating InP(Fe), *p*-type InP(Zn), undoped InP, and also for *n*-type GaP. The only apparent variations in the SIMS spectra occur for the undoped and lowly doped substrates where a slightly higher Mn concentration is found away from the surface beyond 200 nm. It is concluded that the specifics of the substrate doping have little influence on the segregation process.

C. STEM

In Fig. 3(a), the STEM image taken on a Mn-implanted (3×10^{16} cm^{-2}) InP (undoped) substrate and annealed for 60 s at 650 °C reveals that the implanted layer after annealing contains a significant number of defects, but nevertheless it remains epitaxially coherent with the underlying substrate. To determine the actual location of the principal atoms, EDS mapping of In, Mn, and P was carried out over the area

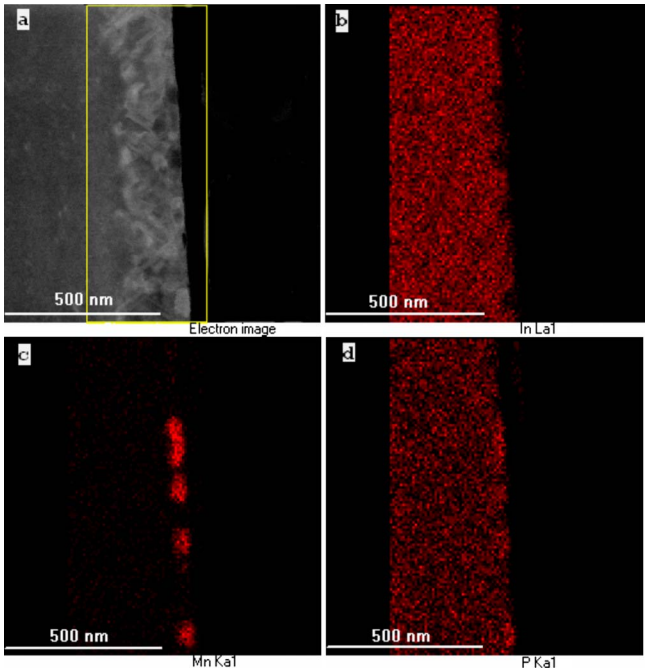

FIG. 3. (Color online) (a) STEM image of an InP (undoped) implanted with Mn (3×10^{16} cm^{-2}) and annealed at 650 °C for 60 s; the rectangle represents the area used for the EDS, chemical mapping of (b) In ($L\alpha_1$), (c) Mn ($K\alpha_1$), and (d) P ($K\alpha_1$).

defined in Fig. 3(a). The results shown in Figs. 3(b)–3(d), respectively, are obtained using the principal x-ray emissions generated by the electron beam. Most of the Mn is located at the surface in ovoid clusters having a mean size of 60 nm [Fig. 3(c)]. This finding is in very good agreement with the SIMS and RBS measurements presented in Secs. III A and III B. In addition, Figs. 3(b) and 3(d) reveal that the Mn-rich areas are also rich in P and depleted in In, suggesting the formation of a Mn–P compound.

Electron diffraction on the implanted layer shows the [110] pattern of the InP matrix and also several much weaker diffraction spots that can be indexed as MnP (001), (310), and (021) diffractions [marked with arrows in Fig. 4(a)]. The (001) diffraction in MnP is normally forbidden; its appearance for this sample is consistent with a defective or constrained structure with possible deviations from stoichiometry. Furthermore, there is no indication in the diffraction pattern of rings specific to polycrystalline material, suggesting the presence of a single grain or grains with a limited number of specific orientations.

The high resolution image of a region at the surface highly concentrated in Mn, as shown in Fig. 4(b), was taken with the electron beam oriented along the [110] direction of the substrate. In the photo at least two different sets of MnP (110) lattice planes (d=3.93 Å) can be distinguished, indicating a polycrystalline rather than a monocrystalline structure.

D. VSM

Magnetic moment measurements down to 100 K on the as-implanted samples indicate only a diamagnetic response that is indistinguishable from the diamagnetic signal of the

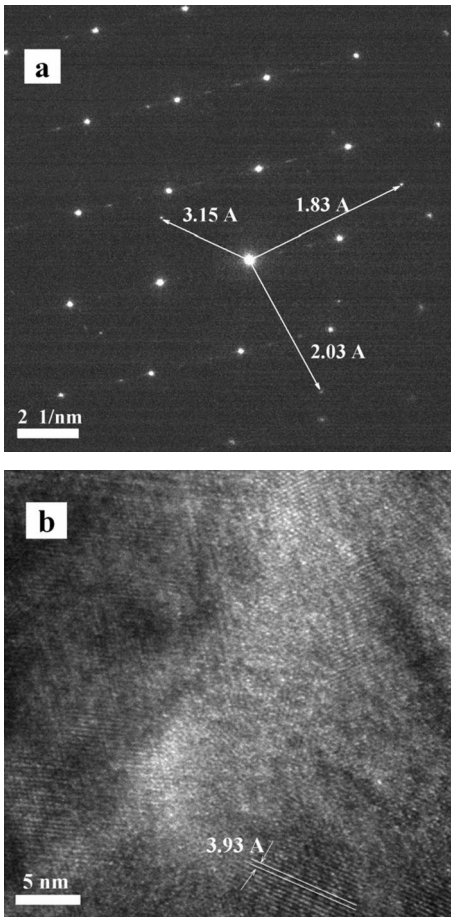

FIG. 4. (a) Electron diffraction pattern from an area of the Mn-implanted InP layer. The arrows indicate MnP crystal diffractions; (b) high resolution image on a Mn- and P-rich regions of the sample presented in Fig. 3.

substrate. After annealing above 600 °C, all implanted InP samples as well as the implanted GaP show an additional ferromagnetic contribution. Figure 5 presents the hysteresis curves, after subtraction of the diamagnetic background signal, at 100 K for the magnetic field oriented along two principal directions of the cubic InP(S):Mn material.

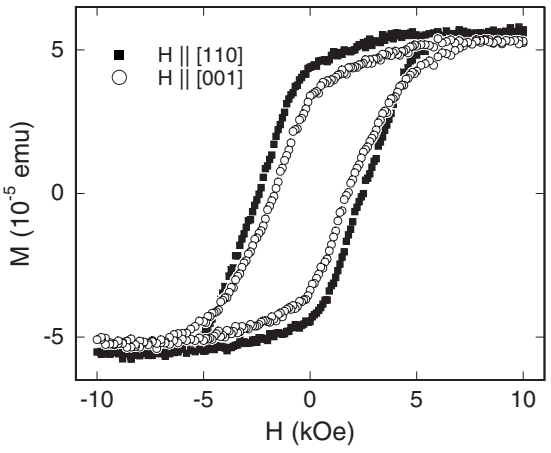

FIG. 5. Hysteresis loops at 100 K of an InP(S) sample implanted with Mn (5×10^{16} cm^{-2}) and annealed at 650 °C for 1 min as measured with the applied field oriented along the [110] and [001] directions of the InP substrate.

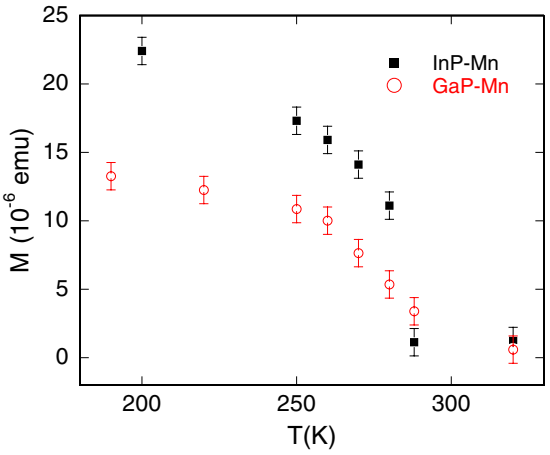

FIG. 6. (Color online) The variation in the magnetic moment with temperature for InP(S):Mn and GaP(S) samples, both Mn implanted to a fluence of 3×10^{16} cm^{-2}. These measurements were obtained with a field of 5 kOe oriented along the [110] substrate direction.

The shape of the hysteresis loop is observed to vary at constant temperature with the field orientation, that is to say, there is a variation of order 25%–30% in the remanence, the coercivity, and the saturation field, whereas the saturation moment remains nearly isotropic. It should be noted that all moment measurements in nonzero magnetic fields are dominated by the large diamagnetic contribution of the InP (or GaP) substrate material. Given the uncertainties in the substrate susceptibility, it is possible that the subtraction masks the fact that the Mn moment does not reach complete saturation at the fields available.

The high coercivities (H_c=2375 Oe$\|$[110] and 1850 Oe$\|$[001]) shown in Fig. 5 are typical of samples measured at this temperature. As a function of the temperature, the coercivity$\|$[110] rises rapidly from about 280 to 200 K, below which temperature it levels off above 2 kOe. Similar anisotropic behavior has been found for the GaP:Mn material. In MOCVD-grown GaP:Mn samples,[14,15] a nearly identical anisotropy of the hysteresis loop has been related to structural texturing wherein embedded MnP particles are oriented preferentially with respect to the III-V host matrix.

Ferromagnetic materials with large coercivities often show divergences between zero-field-cooled (ZFC) and field-cooled (FC) M-T curves. For the present implanted materials, such divergences have been observed for applied fields less than H_c. However, the differences disappear above 280 K so that the ZFC and FC curves coincide from this point to well above the Curie temperature (T_C). In order to determine the value of T_C, the magnetic moment at constant applied field has been measured as a function of temperature. Figure 6 shows data for both InP(S):Mn and GaP(S):Mn measured at 5 kOe. Extrapolating the magnetic moment to zero gives $T_C=290\pm3$ K. This range applies to all annealed samples measured to date.

IV. DISCUSSION AND CONCLUSION

A clear picture emerges from these results. Initial implantation of 200 keV Mn ions at fluences above 10^{16} cm^{-2} causes an amorphization of the substrate to depths of 320 nm. This amorphous layer shows no collective magnetism, giving only a diamagnetic signal for temperatures above 100 K. Annealing above 600 °C results in an epitaxial recrystallization of the layer and a significant segregation of the implanted Mn to a region about 60 nm wide at the surface. Since this same region is depleted in In and enhanced in P, the formation of a Mn–P compound is suggested, in which electron diffraction measurements identify as binary MnP. Magnetic data support this conclusion.

MnP is a ferromagnetic compound with an orthorhombic crystal structure and very strong magnetic anisotropy.[17] Its Curie temperature of 291.5 K corresponds exactly, within experimental uncertainties, to that found for all the implanted and annealed samples studied here [Fig. 5(b)]. The magnetic anisotropy axes correspond to the crystallographic directions ($a>b>c$) and follow the same order with the c-direction being the easy magnetic axis. The magnetic anisotropy of the implanted and annealed samples, implied by the high coercivity, adds further confirmation of the formation of nanometer-sized MnP particles in these materials.

The magnetic moment data at 200 K can be inverted to provide an estimate of the minimum fraction of the implanted Mn that is captured into the MnP particles. Huber and Ridgley[17] reported a magnetic moment per Mn atom in MnP of $(1.29\times0.8)=1.03\mu_B$ at 200 K. Using the value of 2.24×10^{-5} emu indicated in Fig. 6 gives 2.34×10^{15} Mn atoms for this sample with area 25 mm^2. Thus, 9.4×10^{15} Mn atoms cm^{-2} or 31% of the implanted Mn has been transformed into embedded MnP particles. This estimate of the number of Mn atoms, which is typical of all the samples measured, represents the minimum value for two reasons. First, the dominant diamagnetism of the substrate may mask additional contributions for applied fields beyond the point where the hysteresis loop closes. Second, the strong magnetic anisotropy of MnP may render a complete saturation of the magnetic moment difficult for fields not in the magnetically easy c-direction.

MnP particles in the implanted material are situated exclusively at the surface of the InP and GaP materials, with grain sizes ~10 nm [Fig. 4(b)]. Microscopy measurements have not as yet established a definitive texture with respect to the substrate for these grains. In comparison, the MnP particles embedded in GaP, grown by MOCVD,[14,15] are distributed uniformly throughout the layers and are much larger (~50 nm). Moreover, these particles are clearly observed to grow with a definite texture in which the MnP c-axis aligns preferentially along the [110] directions of the III-V host lattice.

In spite of these differences, the magnetization behavior of the two types of material is very similar at all temperatures studied. This observation opens the possibility that the texture detected in the MOCVD-grown material may also be present in the implanted and annealed layers described in this study. Supporting evidence for this speculative conclusion can be found in the observed anisotropy of the magnetic remanence and coercivity of the two materials.

ACKNOWLEDGMENTS

We would like to acknowledge helpful discussions with David Ménard, Patrick Desjardins, and Remo Masut about their MOCVD-grown GaMnP samples. In addition we thank Martin Chicoine, Louis Godbout, and Louis-Philippe Carignan for their assistance with the ion implantation and the VSM measurements. This research has been supported by NSERC, Canada and FQRNT, Quebec.

[1]H. Ohno, A. Shen, F. Matsukura, A. Oiwa, A. Endo, S. Katsumoto, and Y. Iye, Appl. Phys. Lett. **69**, 363 (1996).
[2]H. Ohno, H. Munekata, T. Penney, S. von Molnar, and L. L. Chang, Phys. Rev. Lett. **68**, 2664 (1992).
[3]F. Matsukura, H. Ohno, A. Shen, and Y. Sugawara, Phys. Rev. B **57**, R2037 (1998).
[4]M. A. Scarpulla, B. L. Cardozo, R. Farshchi, W. M. Hlaing Oo, M. D. McCluskey, K. M. Yu, and O. D. Dubon, Phys. Rev. Lett. **95**, 207204 (2005).
[5]Y. Shon, H. C. Jeon, Y. S. Park, W. C. Lee, S. J. Lee, D. Y. Kim, H. S. Kim, H. J. Kim, T. W. Kang, Y. J. Park, C. S. Yoon, and K. S. Chung, Appl. Phys. Lett. **85**, 1736 (2004).
[6]T. Dietl, H. Ohno, F. Matsukura, J. Cibert, and D. Ferrand, Science **287**, 1019 (2000).
[7]S. Das Sarma, E. H. Hwang, and A. Kaminski, Phys. Rev. B **67**, 155201 (2003).
[8]M. Berciu and R. N. Bhatt, Phys. Rev. Lett. **87**, 107203 (2001).
[9]G. A. Prinz, Science **250**, 1092 (1990).
[10]Y. D. Park, J. D. Lim, K. S. Suh, S. B. Shim, J. S. Lee, C. R. Abernathy, S. J. Pearton, Y. S. Kim, Z. G. Khim, and R. G. Wilson, Phys. Rev. B **68**, 085210 (2003).
[11]Y. Shon, H. C. Jeon, Y. S. Park, S. J. Lee, D. Y. Kim, H. S. Kim, T. W. Kang, Y. J. Park, C. S. Yoon, C. K. Kim, E. K. Kim, Y. Kim, and Y. D. Woo, J. Cryst. Growth **281**, 501 (2005).
[12]M. E. Overberg, B. P. Gila, C. R. Abernathy, S. J. Pearton, N. A. Theodoropoulou, K. T. McCarthy, S. B. Arnason, and A. F. Hebard, Appl. Phys. Lett. **79**, 3128 (2001).
[13]M. L. Reed, N. A. El-Masry, H. H. Stadelmaier, M. K. Ritums, M. J. Reed, C. A. Parker, J. C. Roberts, and S. M. Bedair, Appl. Phys. Lett. **79**, 3473 (2001).
[14]S. Lambert Milot, C. Lacroix, D. Menard, R. A. Masut, P. Desjardins, M. Garcia-Hernandez, and A. de Andres, J. Appl. Phys. **104**, 083501 (2008).
[15]C. Lacroix, S. Lambert Milot, P. Desjardins, R. A. Masut, and D. Ménard, J. Appl. Phys. **103**, 07D531 (2008).
[16]Y. Shon, S. Lee, H. C. Jeon, S.-W. Lee, D. Y. Kim, T. W. Kang, E. K. Kim, D. J. Fu, X. J. Fan, C. S. Yoon, and C. K. Kim, Appl. Phys. Lett. **88**, 232511 (2006).
[17]E. E. Huber, Jr. and D. H. Ridgley, Phys. Rev. **135**, A1033 (1964).
[18]A. Katz, *Indium Phosphide and Related Materials: Processing, Technology and Devices* (Artech House, Boston, London, 1992).
[19]J. S. Williams, Mater. Sci. Eng., A **253**, 8 (1998).
[20]J. F. Ziegler, J. P. Biersack, and U. Littmark, *The Stopping and Range of Ions in Solids* (Pergamon, New York, 1985).
[21]L. R. Doolittle, Nucl. Instrum. Methods Phys. Res. B **15**, 227 (1986).
[22]J. S. Custer, A. Polman, and H. M. van Pinxteren, J. Appl. Phys. **75**, 2809 (1994).